Chapter 5

Seamless Mode Control Algorithm for a Single-Stage Photovoltaic Virtual Synchronous Generator for Frequency Regulation and Reactive Power Support

5.1 Introduction

Photovoltaic (PV) systems require an inverter to deliver the AC output power to the distribution grid, which doesn't offer much inertia. Low penetration of PV inverters into the power grid doesn't affect the stability of the power system. However, the increasing penetration of PV inverters reduces the overall inertia of the power system. Hence, PV systems stability is reduced. VSG control offers a good solution to virtual inertia for grid-connected PV systems.

PV system may be two-stage or single stage. Many two-stage grid-connected PV systems are discussed in Section 1.7.4. A two-stage PV system generally incorporates BESS and the DC-DC converter that adds additional costs. Hence, a single stage PV system is proposed in this chapter. The grid integration of PV-VSG, requires a PLL. However, a self-synchronization method has been used in this work that offer fast, accurate, and

effortless synchronization of PV inverters.

Also, PV systems usually run in MPPT mode to extract the maximum power production. So, they can not absorb or release more power in the events of frequency transients due to a lack of power reserves. Hence, PV-VSG working at MPPT does not participate in frequency regulation. Hence, the concept of the power reserve is presented in this work. Also, the conventional PV system requires a separate controller for STATCOM operation, which is addressed in this chapter.

This chapter presents a single-stage self-synchronized PV-VSG with a seamless mode control (SMC) algorithm to provide ancillary support to the grid frequency disturbances by maintaining power reserve and also working as a STATCOM during the unavailability of PV power. The major contributions of this work are:

- It eliminates the requirement for the storage element to provide frequency support.
- The proposed PV-VSG works in self-synchronizing mode. Hence, there is no need for PLL for the grid synchronization.
- It can supply the non-linear loads without using any additional harmonics compensation methods.
- The proposed PV-VSG is able to shift seamlessly from grid-tied mode to islanded mode in the event of grid faults during the day.
- During the nighttime, PV-VSG works as a STATCOM to support the reactive power demands. No separate control algorithm is required for the STATCOM operation to maintain DC link voltage.

The experimental setup of PV-VSG is implemented in the laboratory and verified to ensure the viability of the proposed system. The performance of the proposed SMC controller under various cases is presented through experimental results.

A brief outline of the chapter is as follows:

- Section 5.2 describes the structure of the single-stage PV-VSG.
- The proposed seamless mode control (SMC) algorithm of PV-VSG is presented in 5.3.

- PV-VSG controller is presented in 5.4.
- The experimental results are covered in section 5.5.
- The conclusion is made in section 5.6.

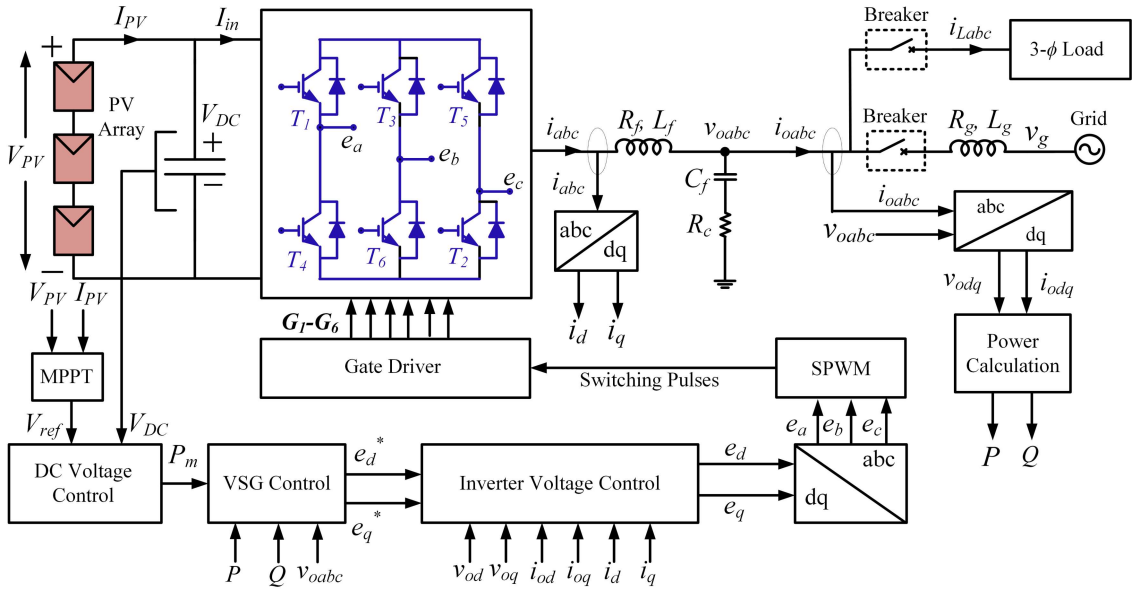

Figure 5.1: Block diagram of a conventional single-stage photovoltaic virtual synchronous generator

5.2 Structure of Single-Stage PV-VSG

The structure of a 3-phase grid-connected PV-VSG system is shown in Figure 5.1. The PV-VSG system consists of the power part and the control part. The power part of the system consists of a PV array and a 3-ϕ inverter. The PV array and inverter are connected through a DC-link capacitor. LC filter is used for the filtering of the switching harmonics. I_{PV}, V_{PV}, and I_{in} denote the PV current, PV voltage, and inverter current, respectively.

5.3 Control Algorithm

The complete control scheme is shown in Figure 5.2. Details of each part of control algorithm is discussed in the following subsections.

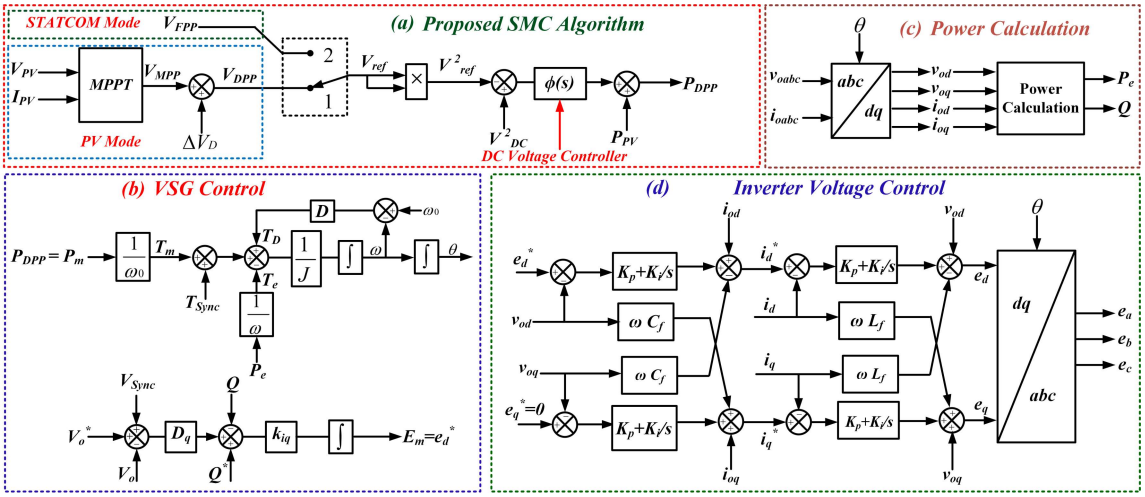

Figure 5.2: SMC algorithm of single-stage photovoltaic virtual synchronous generator

5.3.1 VSG Controller

VSG control equations embody the synchronous generator's attributes, such as kinetic inertia and damping. The following equations (5.1) and (5.2) describe the VSG control.

$$T_m - T_e + D(\omega_0 - \omega) = J\frac{d\omega}{dt} \tag{5.1}$$

$$\sqrt{2}E = k_{iq}\int (Q^* - Q) + \sqrt{2}D_q(V^*{}_o - V_o) \tag{5.2}$$

(5.1) and (5.2) outline the VSG's active and reactive power controllers, respectively. D and J stand for virtual damping and virtual inertia, respectively. The reference torque given to VSG is T_m, and the torque produced by VSG is T_e. VSG frequency and rotor angle are ω (rad/sec) and θ, respectively. ω_0 (rad/sec) stands for the reference frequency of VSG. P_m and P_e stand for reference active power and VSG active power, respectively. V_o* represents the output voltage reference, and V_o is the VSG output voltage. E specifies the generated voltage reference. The parameter k_{iq} is an integral gain, and D_q helps to regulate reactive power according to the voltage variation in the grid. Q^* is the reactive power reference given to the VSG, and Q is the reactive power supplied by the VSG. In this article, a synchronizing torque and voltage-based self-synchronizing method is used for grid synchronization. The synchronizing torque is estimated as given in (5.3)

$$T_{Sync} = k_{Sync}(v_{g\alpha}v_{o\beta} - v_{g\beta}v_{o\alpha}) \tag{5.3}$$

Where $v_{g\alpha}$, $v_{g\beta}$, $v_{o\alpha}$ and $v_{o\beta}$ are $\alpha\beta$ components of grid and VSG voltage respectively. k_{Sync} is a gain. Similarly, the synchronizing voltage signal is calculated as given in (5.4)

$$V_{Sync} = \sqrt{(V_{g\alpha}^2 + V_{g\beta}^2)} - \sqrt{(V_{o\alpha}^2 + V_{o\beta}^2)} \tag{5.4}$$

T_{Sync} is changed accordingly to make $\theta_o = \theta_g$. Similarly, V_{Sync} will make the $V_o = V_g$.

5.3.2 DC Voltage Controller

DC link voltage is maintained to operate at a particular point. Hence, a DC link voltage controller is employed. Reference voltage V_{ref} to the controller is determined by MPPT or non-MPPT mode control of PV. The DC voltage compensator $\phi(s)$ is designed to generate reference power P_m for the VSG algorithm. The DC voltage controller structure is as follows:

$$\phi(s) = \frac{G_0}{s}\frac{(s+n)^2}{(s+d)^2} \tag{5.5}$$

Where n and d are the poles and zeroes of the compensator. Here, the higher-order compensator is used to provide enough phase margin. $\phi(s)$ provides the reference real power P_m to the VSG controller as:

$$P_m = P_{PV} + \phi(s) \tag{5.6}$$

5.3.3 Proposed Seamless Mode Control (SMC) Algorithm

5.3.3.1 Mode of Operation

The preferred operating mode of the PV system is PV mode, i.e., active power generation. However, the PV source can only generate active power during the daytime. Solar irradiance is at its peak for around 5 hours from 11 a.m. to 4 p.m. Hence, the PV-VSG system can not work entirely in PV mode, i.e., it needs to shift the operating mode according to the availability of the PV power. The PV-VSG system works in PV mode during the day to supply active power and participate in frequency regulation. But, when the PV power generation is low or zero (nighttime), the PV-VSG system doesn't utilize the inverter capacity. So, the PV-VSG system operates entirely in the STATCOM mode during nighttime to provide reactive power support to the grid. The PV-VSG system can also work in STATCOM mode during the daytime if required. Hence, two operating

modes of the proposed PV-VSG system are:
(1) PV mode (2) STATCOM mode.

5.3.3.2 PV Mode Operation

During the daytime, the PV system works in PV mode, i.e., PV generates the real power and may participate in frequency regulation. However, if the photovoltaic systems operate at the maximum power point, irrespective of the load condition, the PV will give a fixed maximum output for the fixed amount of irradiance and temperature. Hence, PV cannot contribute to the frequency control in this case. This happens due to the unavailability of the reserve power with PV to participate in frequency control. Hence, it is desirable to always maintain some power reserve in the PV systems, which is obtained by operating the PV system at the deloaded MPPT condition, i.e., less than MPPT power. To operate

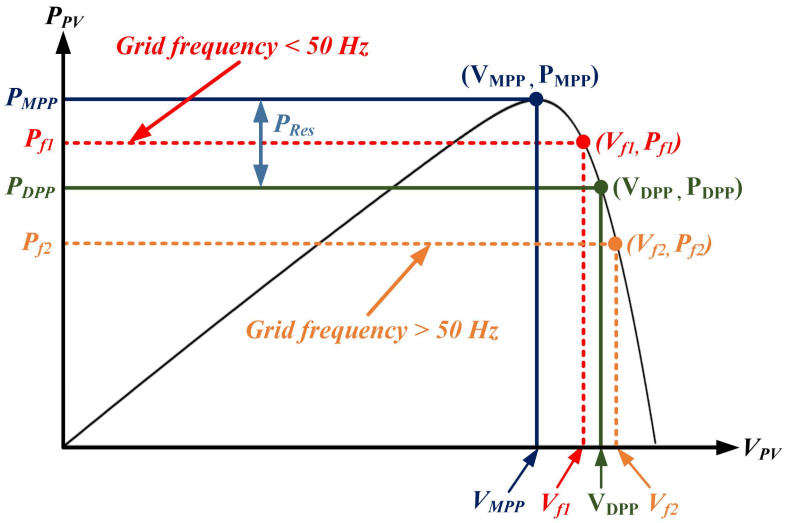

Figure 5.3: Power reserve in PV-VSG

at the deloaded power, PV output voltage should be either higher or lower than MPPT voltage, i.e., PV needs to operate either on the left or right side of the MPPT point on the PV curve. However, the slope of the PV curve on the right side of MPPT is steeper than on the left. Also, the PV system is unstable at the left side of the MPPT point. Hence, operating the PV at more than MPPT voltage is preferable. The concept of power reserve is explained in the Figure 5.3.

Here, P_{MPP} denotes the maximum power output of the PV array, and V_{MPP} refers to the PV output voltage at the maximum power point. V_{DPP} is the PV output voltage

beyond V_{MPP} or the PV voltage corresponding to the deloaded power. P_{DPP} represents the deloaded power at V_{DPP}. If the PV-VSG is operated at P_{DPP}, then PV doesn't extract the maximum power output, and there is some extra power remaining, which can be used for ancillary support such as frequency regulation. This extra power is denoted as P_{Res}. Hence, $P_{Res} = P_{MPP} - P_{DPP}$.

5.3.3.3 Proposed SMC Controller for Frequency Regulation (PV Mode)

The proposed SMC control algorithm is depicted in Figure 5.2 (a). Here, switch 1 is closed. To operate PV at DPP, PV voltage is increased beyond the V_{MPP} point, i.e., V_{DPP} as shown in Figure 5.3. Difference between the V_{MPP} and V_{DPP} is denoted by ΔV_D. In case of frequency changes in the grid, PV will be asked to generate either more power or less power depending on the increment or decrement in the grid frequency. VSG has an inherent frequency control mechanism. The term $D(\omega_0 - \omega)$ in (5.1) corresponds to the active power due to the frequency mismatch between VSG and the grid. So, when the grid frequency is 50 Hz, then the term $D(\omega_0 - \omega) = 0$. If the grid frequency is less than 50 Hz, then $D(\omega_0 - \omega) > 0$ and PV will inject more power to the grid than P_{DPP}, and the operating point will be (P_{f_1},V_{f_1}) as shown in Fig. 5.3. Similarly, if the grid frequency is more than 50 Hz, then $D(\omega_0 - \omega) < 0$ and PV will inject lesser power to the grid than P_{DPP} and the operating point will be (P_{f_2}, V_{f_2}). So, PV-VSG will automatically control the power due to the grid frequency variation. Complete PV-VSG Controller with SMC algorithm and VSG control is depicted in Figure 5.2.

5.3.3.4 Proposed SMC Controller in STATCOM Mode

During the daytime, when solar irradiance is available, PV-VSG works in the PV mode, either in standalone or grid-connected mode, depending on the PV power generation. Hence, it supplies active power and participates in the frequency regulation services. But, during the night, solar irradiance is zero. So, the inverter of the PV-VSG system might be under-utilized. Hence, PV-VSG is transferred to the STATCOM mode during night hours. Power generation by the PV source is zero at this time. Therefore, DC link voltage is maintained by the STATCOM mode operation of the PV-VSG system. So, switch 2 in Figure 5.2 (a) is closed, and switch 1 is opened. Now, the reference voltage to the DC voltage controller is V_{FPP} instead of V_{DPP}. V_{FPP} is a constant DC reference voltage equal

to the open circuit voltage of the PV array. The only difference for both the operating modes is the reference DC voltage. The same DC voltage controller maintains the DC link voltage during the PV and STATCOM modes. Hence, there is no need for a separate control algorithm for the STATCOM operation of PV-VSG.

5.4 Controller Design

The small signal model of VSG control is derived as [51],

5.4.1 VSG Controller

The active and reactive power output of VSG can be represented as:

$$P = \frac{3V_o V_g sin\delta}{X_g} \tag{5.7}$$

$$Q = \frac{3V_o}{X_g}(V_o - V_g cos\delta) \tag{5.8}$$

Here, X_g is the grid-side reactance. The transfer function of VSG by small signal perturbation can be derived as [51]:

$$\frac{\hat{T_e}(s)}{\hat{\delta}(s)} = \frac{3V_{on}V_{gn}}{X_g\omega_n} \tag{5.9}$$

$$\hat{\delta}(s) = \frac{\hat{\omega}(s) - \hat{\omega_g}(s)}{s} \tag{5.10}$$

$$\frac{\hat{Q(s)}}{\hat{V_o(s)} - \hat{V_g(s)}} = \frac{3V_{on}}{X_g} \tag{5.11}$$

Where V_{on} and V_{gn} are the nominal values of the VSG and grid voltage, respectively. VSG control consists of real power and reactive power loops, as in (5.1) and (5.2). The design part of the VSG active and reactive power control loop is explained below:

5.4.1.1 Active Power Controller

From (5.1), the small signal transfer function of active power can be derived as follows:

$$\frac{\hat{\omega(s)}}{\hat{T_m}(s) - \hat{T_e}(s)} = \frac{1}{Js + D} \tag{5.12}$$

The loop transfer function of the active power controller in (5.9) and (5.12) can be written as:

$$G_p(s) = \frac{\hat{P}_m}{\hat{P}_e} = \frac{3V_{on}V_{gn}}{X_g\omega_n s}\frac{1}{Js+D} \tag{5.13}$$

Here, J and D are designed to achieve proper phase margin and gain margin. The damping coefficient D is designed by the grid code. After designing D, J is designed to maintain stability and keep the loop gain at power line frequency to a minimum to ensure good disturbance rejection. Hence, the bandwidth and phase margin of the VSG active power loop are designed for 22 Hz and 34.7^0, respectively. Figure 5.4 depicts the Bode plot of the active power loop of VSG.

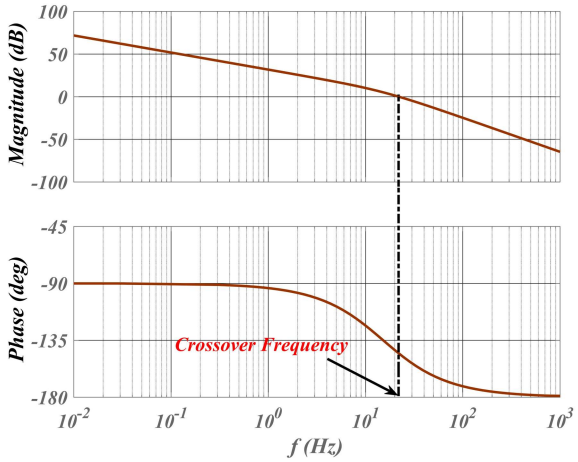

Figure 5.4: Bode plot of VSG active power controller

5.4.1.2 Reactive Power Controller

From (5.2), the small signal transfer function of reactive power can be derived as:

$$\frac{\hat{E}_m(s)}{\hat{Q}^*(s) - \hat{Q}(s)} = \frac{k_{iq}}{\sqrt{2}}\frac{1}{s + D_q k_{iq}} \tag{5.14}$$

The loop transfer function of the VSG reactive power controller from (5.11) and (5.14) can be written as:

$$G_q(s) = \frac{3V_{on}}{X_g\sqrt{2}}\frac{k_{iq}}{s + D_q k_{iq}} \tag{5.15}$$

k_{iq} and D_q are designed to fulfill the stability criterion. The reactive power loop is designed for a 105^0 phase margin. D_q is designed according to the reactive power regulation

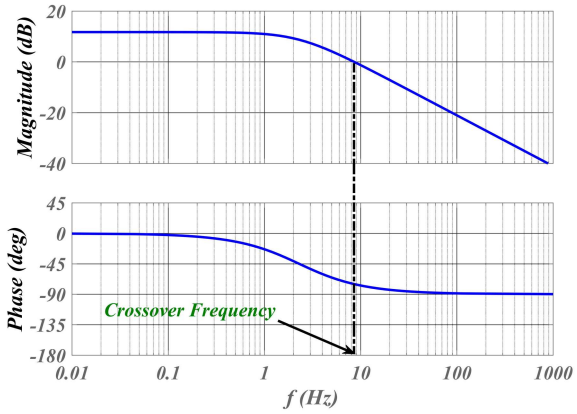

Figure 5.5: Bode plot of VSG reactive power controller

requirements. k_{iq} is the integrator gain and decides the speed of the reactive power controller. The reactive power controller of VSG is designed for a bandwidth of 8 Hz. Figure 5.5 illustrates the bode diagram of the reactive power controller.

5.4.2 DC Voltage Controller

After designing the inner VSG controller, the outer loop DC voltage controller is designed. From the PV power balance, the dc-link voltage equation ignoring the losses can be derived as:

$$\frac{C_{DC}}{2}\frac{dV_{DC}^2}{dt} = P_{PV} - P_{in} \tag{5.16}$$

Where V_{DC} is the sensed DC voltage and C_{DC} is the capacitance of the DC link capacitor. If the switching losses of the inverter are ignored, then $P_{in} = P_g$. Where P_{in} is the inverter input power, and P_g is power injected into the grid. So,

$$\frac{C_{DC}}{2}\frac{dV_{DC}^2}{dt} = P_{PV} - P_g \tag{5.17}$$

(5.17) indicates that a mismatch between PV output power (P_{PV}) and power injected into the grid (P_g) leads to an imbalance in the DC link voltage. Hence, to regulate the power injected into the grid (P_g), the DC link voltage controller provides the reference signal (P_m) to the VSG controller.

Here, PV power (P_{PV}) is used as a feedforward term. So, by linearizing the (5.17) as given in [146], the relation between variation in DC voltage with respect to the grid

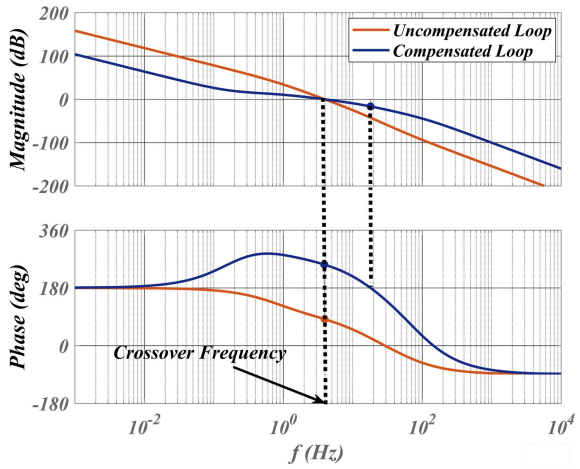

Figure 5.6: Bode plot of DC voltage loop

power is given by:

$$G_{VP}(s) = \frac{\hat{V}_{DC}^2(s)}{\hat{P}_g(s)} = \frac{-4LsP_{PV0} - 6V_{od}^2}{3sC_{DC}V_{od}^2} \tag{5.18}$$

Where P_{PV0} is the steady state value of PV power and L is the equivalent inductance. The closed-loop DC voltage controller is composed of compensator $\phi(s)$, VSG active power controller $G_p(s)$, and the control plant $G_{VP}(s)$. Hence, the loop transfer function for the DC link voltage control loop is written as follows:

$$G_{DC(s)} = -\phi(s)G_p(s)G_{VP}(s) \tag{5.19}$$

Here, -1 is multiplied to make up for the negative sign of G_{VP}. The controller design takes care of the extreme case (negative rated PV power). Since the design requirements can not be achieved with the first-order compensator, a second-order compensator for DC voltage control has been designed. The bandwidth of the DC voltage controller is chosen around 3.95 Hz, i.e., smaller than the inner VSG controller. To achieve the desired gain crossover frequency of 3.95 Hz, a DC gain is added. The phase margin is very poor, around -97.5^0 without a compensator. Hence, a second-order compensator with phase lead compensation is designed to make the control loop stable with a 72.9^0 phase margin. Figure 5.6 depicts the bode diagram of the DC voltage controller.

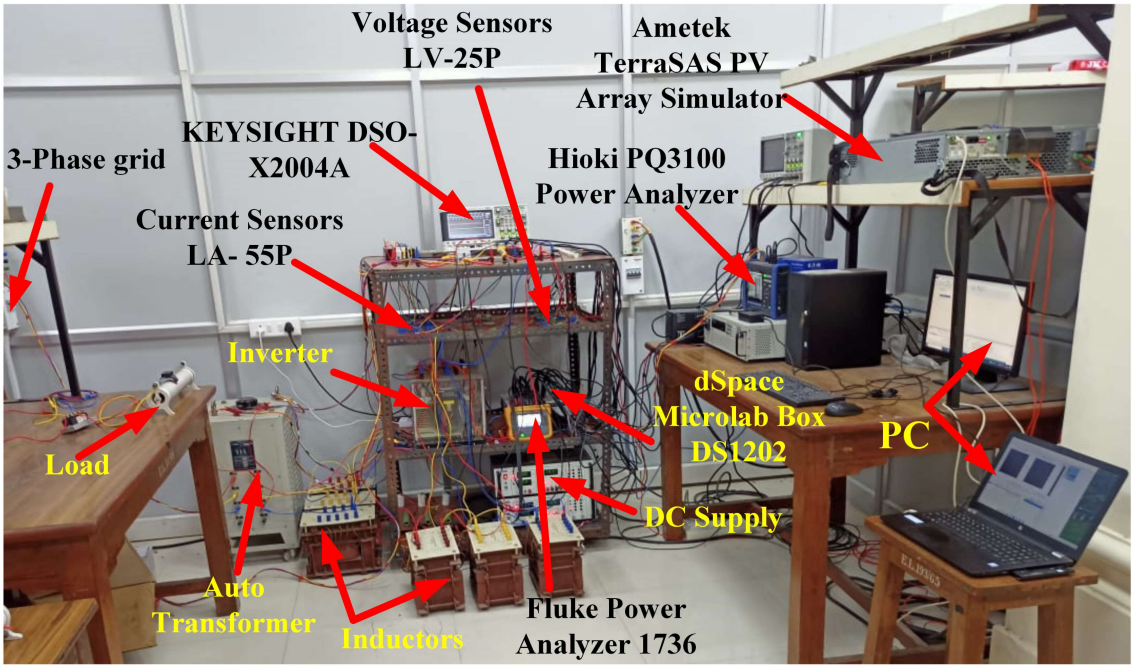

Figure 5.7: Hardware prototype

5.5 Experimental Results

To verify the proposed SMC algorithm, a laboratory prototype of the PV-VSG system was developed, as shown in Figure 5.7. The PV simulator TerraSAS is used to emulate the power characteristics of a PV array. PV-VSG parameters used in the experiment are given in the Table 5.1, Table 5.2 and Table 5.3. The proposed SMC algorithm was tested with different irradiance and frequency regulation cases during the daytime when PV-VSG is working in PV mode. Also, the STATCOM mode of the PV-VSG system is tested at night times when the PV power is not available. Experimental results validate the performance of the proposed PV-VSG under different test cases.

5.5.1 PV Mode

5.5.1.1 Steady-State Performance at $G = 1000w/m^2$

Initially, the PV array is tested with the proposed SMC algorithm for the fixed irradiance $G = 1000w/m^2$. Figure 5.8(a), 5.8(b), and 5.8(c) show the steady state values of PV-VSG output currents and voltages. Figure 5.9 shows the PV characteristics at DPP point, i.e., less than MPPT. Here, the PV-VSG system is not extracting the maximum power.

Table 5.1: PV Simulator Ratings

S.No.	Parameter	Values
1	Open circuit voltage (V_{oc})	250 V
2	Short circuit current (I_{sc})	5.6 A
3	MPP voltage (V_{MPP})	200 V
4	MPP Current (I_{MPP})	5 A
5	Rated Power (P_{MPP})	1 kW

Table 5.2: Inverter Side Parameters

S.No.	Parameter	Values
1	3-ϕ ac Voltage	110 $V/50$ Hz
2	Interfacing Inductance (L_f)	3 mH
3	Filter capacitance (C_f)	10 μF
4	Filter resistance (R_c)	5 Ω
5	Inverter switching frequency	10 kHz

Table 5.3: VSG Parameters

S.No.	Parameter	Values
1	Virtual Inertia (J)	0.01 $kg - m^2$
2	Virtual damping (D)	1.1
3	k_{iq}	0.045
4	D_q	110 $Var/Volt$

Instead, the power extracted by the PV source is less than MPP power, and the operating point is on the right side of the MPP point in the PV curve, as shown in Figure 5.9. Here, PV-VSG is injecting 800 W real power to the grid. Hence, the PV array still has some reserve power, which can be used in the events of grid frequency variation. As soon as the SMC algorithm is turned on, the PV output voltage starts moving toward the DPP point from the open circuit voltage, and PV-VSG starts injecting active power into the grid. Figure 5.10 shows the PV output voltage, current, and power. Figure 5.11 shows the AC side active and reactive powers and the frequency error between VSG and the

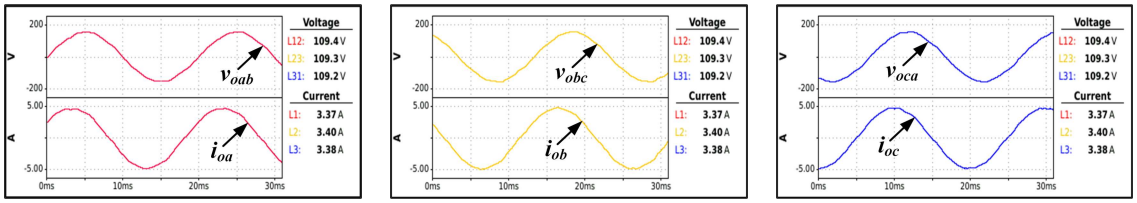

(a) (b) (c)

Figure 5.8: Steady-state VSG voltages and currents (a)$V_{oab} - i_{oa}$(b) $V_{obc} - i_{ob}$ (c) $V_{oca} - i_{oc}$

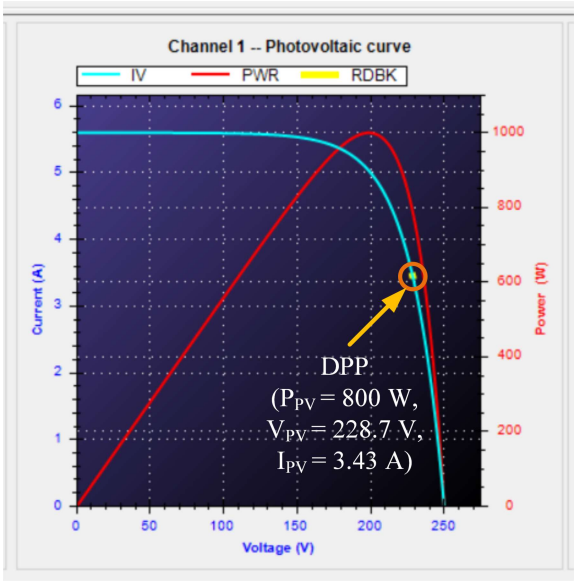

Figure 5.9: DPP point on PV curve for $G = 1000w/m^2$

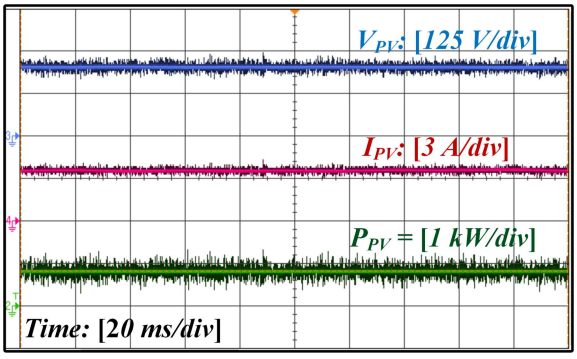

Figure 5.10: V_{PV}, I_{PV} and P_{PV} at $G = 1000w/m^2$

grid (Δf) of the PV-VSG system.

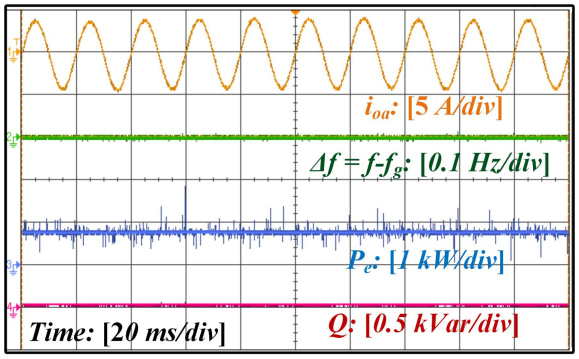

Figure 5.11: i_{oa}, Δf, P_e and Q at $G = 1000 w/m^2$

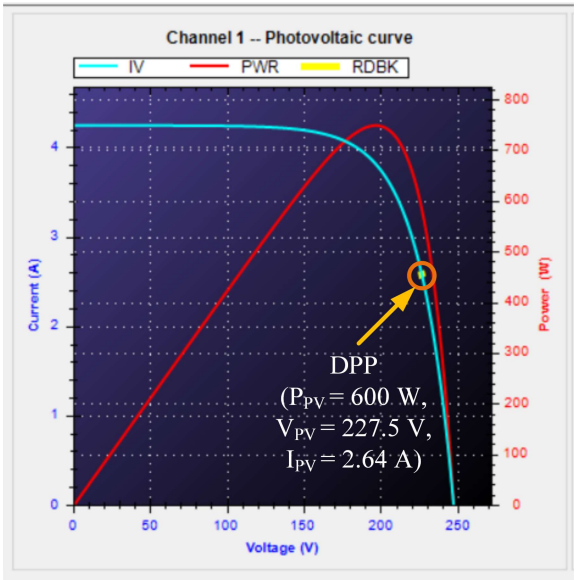

Figure 5.12: DPP point at PV curve for $G = 750 w/m^2$

5.5.1.2 Dynamic Performance with Change in Irradiances (G)

Dynamic performance of the PV-VSG with the proposed algorithm is tested for changing irradiance. Irradiance level is changed from $G = 1000\ w/m^2$ to $G = 750\ w/m^2$. Figure 5.12 shows that the power supplied by the PV array is reduced to 600 W as compared to Figure 5.9. PV array voltage is also slightly changed to 227.5 V from 228.7 V. The DPP point in the PV curve for $G = 750\ w/m^2$ is shown in Figure 5.12.

Dynamics of the PV current (I_{PV}) and power (P_{PV}) are shown in Figure 5.13. As shown in Figure 5.13, the PV current starts decreasing when the irradiance changed to 750 w/m^2. Consequently, power injected into the grid (P_g) is also reduced. Figure 5.14 shows the dynamics of the VSG output powers when G is changed from 1000 to 750 w/m^2.

VSG active power (P) is reduced as soon as the irradiance is changed without affecting the reactive power (Q) flow. Frequency error ($\Delta f = f - f_g$) is zero during irradiance change as the VSG frequency is unaffected. When power changes occur, small frequency

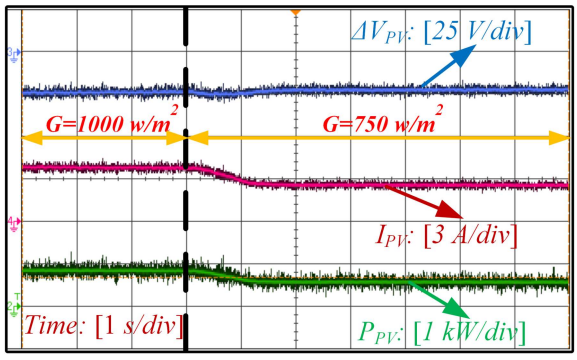

Figure 5.13: Dynamics of PV current and power during changing irradiance, i.e., $G = 1000$ to $750w/m^2$

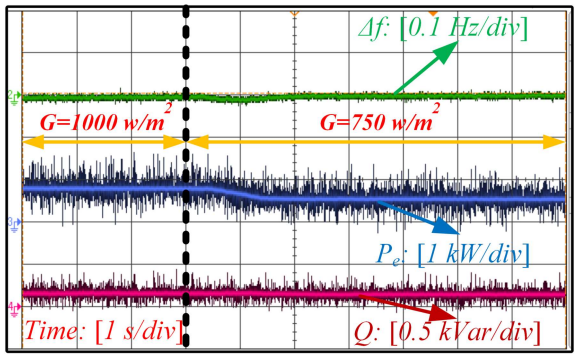

Figure 5.14: Frequency error Δf, active and reactive power during changing irradiance, i.e., $G = 1000$ to $750w/m^2$

transients occur, but that settles quickly.

5.5.1.3 Frequency Regulation Performance

Since we can not change the distribution grid frequency(f_g), the VSG reference frequency is changed to create the frequency difference between VSG and grid frequency. VSG performs the frequency regulation by supplying or absorbing the active power to the grid. PV operating point DPP shifts more towards the MPP point on the PV curve to extract more active power or moves to the right side of DPP to reduce the PV power generation. The change in PV output power when the reference frequency is raised by 0.1 Hz is shown

in Figure 5.15. It is indirectly equivalent to the actual grid frequency being 0.1 Hz less than the reference VSG frequency. At 50 Hz frequency, the PV array output P_{PV} is 850 W as shown in Figure 5.15 (a). Figure 5.15 (b) shows the operating point DPP when the reference frequency goes to 50.1 Hz. Now, the PV power output increases to 950 W. Power exchange due to the frequency difference between PV-VSG and the grid depends on the damping coefficient D. Figure 5.16 (a) shows the dynamics of the PV quantities,

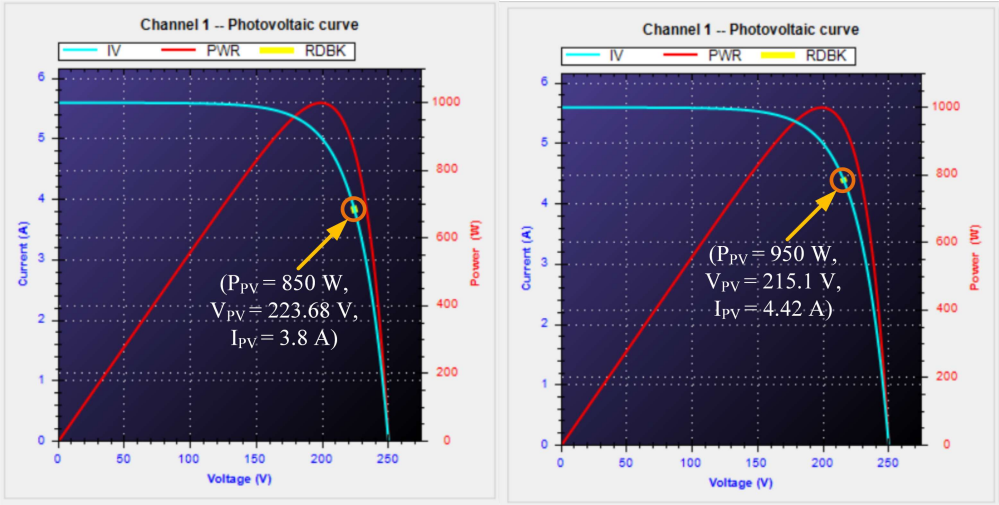

(a) (b)

Figure 5.15: PV operating point when the VSG reference frequency is (a) 50 Hz and (b) 50.1 Hz

i.e., I_{PV} and P_{PV} when the VSG reference frequency changes from 50 Hz to 50.1 Hz. Here, the frequency error (Δf) between VSG and grid frequency is 0.1 Hz, i.e., grid frequency is less than VSG frequency. Hence, the grid demands more active power from the PV system. Here, the power reserve of PV-VSG comes into the picture. Hence, the PV array starts injecting extra power to support the grid, as shown in Figure 5.16 (a). Figure 5.16 (b) shows the dynamics of the VSG output active and reactive power during the reference frequency changes. The active power output of the VSG tends to increase when the VSG frequency changes from 50 to 50.1 Hz. Reactive power Q is unaffected by the grid frequency variation as Q is independent of the frequency.

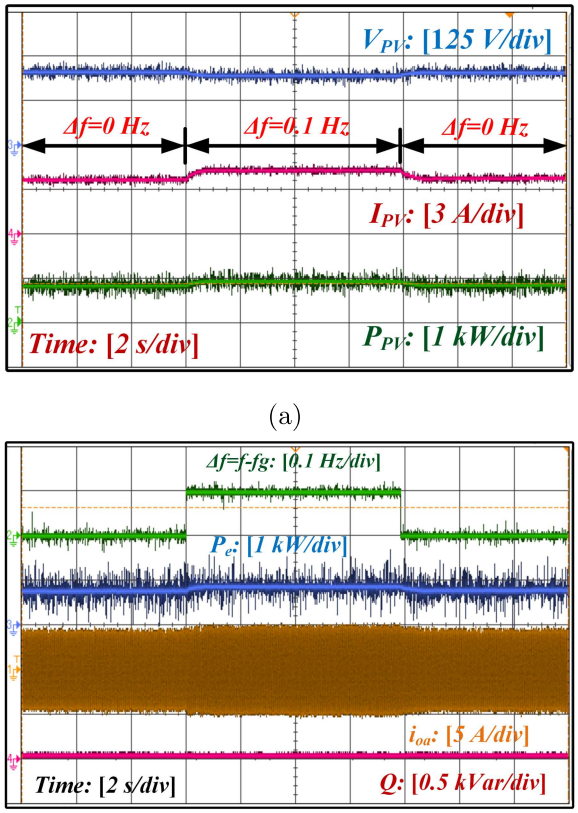

Figure 5.16: Dynamics of the PV-VSG system at (a) PV side and (b) VSG side during frequency variation (Δf) of $0.1Hz$

5.5.1.4 Dynamic Performance with Linear-Load

Single-stage PV-VSG system performance is tested with the linear load. Figure 5.17 shows the VSG voltage v_{oa}, VSG current i_{oa}, load current i_{La} and load power P_L with a constant load. After some time, the load is increased, and the dynamics of the VSG current, load current, and load power are observed. There is a smooth change in the load current and power while the grid current is constant. Hence, the PV-VSG system responds perfectly to the load change. Here the load power P_L is shown negative which indicates that the load is drawing the power.

5.5.1.5 Performance With the Non-Linear Load

Single-stage PV-VSG system performance is tested with the non-linear load. A diode bridge rectifier, as a non-linear load, is connected at the PCC. Figure 5.18 shows the VSG

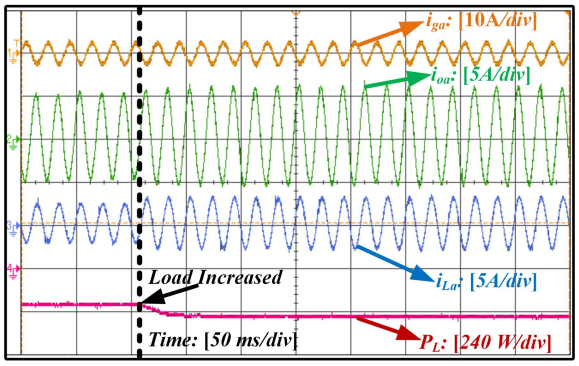

Figure 5.17: Dynamics of grid current i_{ga}, VSG current i_{oa}, load current i_{La} and load power P_L with linear load

voltage, VSG current, load current, and the grid current waveforms for the non-linear load. Grid current is maintained sinusoidal even after the connection of the non-linear load. Hence, PV-VSG supplies the current harmonics requirement of the load without affecting the grid power quality.

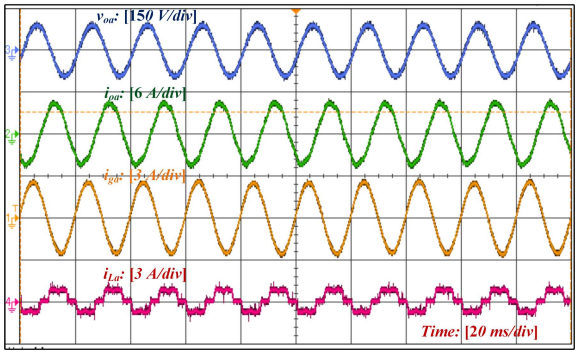

Figure 5.18: Waveforms of VSG voltage v_{oa}, VSG current i_{oa}, grid current i_{ga} and load current i_{La} with non-linear load

5.5.1.6 Seamless Transition from Grid-Connected Mode to Standalone Mode

VSG voltage (v_{oa}), VSG current (i_{oa}), load current (i_{La}) and grid current (i_{ga}) during the transition from grid-interfaced to islanded mode is shown in Figure 5.19. There is a smooth transition in the magnitude of VSG output voltage and load current. During grid-connected mode, some finite amount of grid current i_{ga} was flowing. As soon as the grid is disconnected from VSG, the grid current becomes zero, but load current i_L is still maintained. Hence, there is a seamless transfer of VSG between grid-connected and

islanded modes.

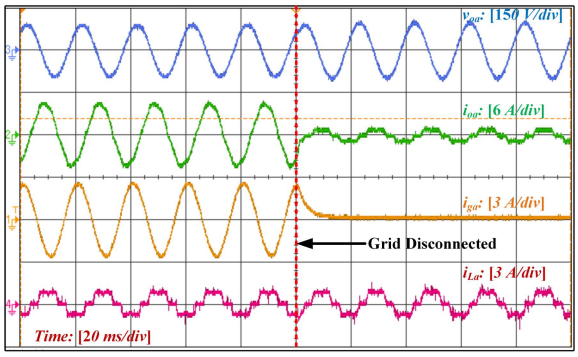

Figure 5.19: Dynamics of VSG voltage v_{oa}, VSG current i_{oa}, grid current i_{ga} and load current i_{La} during the transition from grid-connected to islanded mode

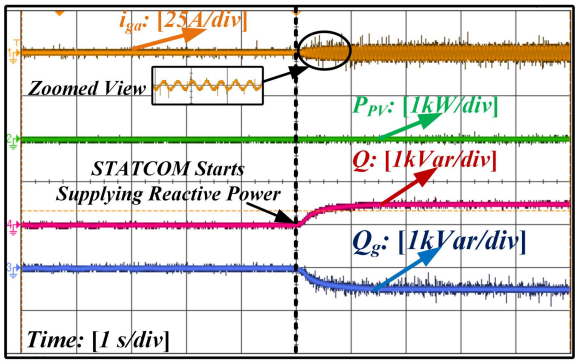

Figure 5.20: Dynamics of i_{ga}, P_{PV}, Q and Q_g during STATCOM mode

5.5.2 STATCOM Mode

During nighttime, PV power generation is zero. Hence, the PV-VSG system starts working in STATCOM mode by opening switch 1 and closing switch 2, as shown in Figure 5.3(a). Figure 5.20 depicts the PV-VSG system performance as a STATCOM. It is observed from Figure 20, that PV power generation is zero because the irradiance $G = 0$ w/m^2 at nighttime. When reactive power is demanded, PV-VSG supplies reactive power to the grid. Figure 5.20 shows that the PV-VSG injects 500 Var reactive power into the grid. Initially, the grid current was zero due to the unavailability of PV power P_{PV}. As soon as the reactive power is supplied to the grid, grid current i_{ga} starts flowing, as shown in Figure 20. Hence, the PV-VSG system works efficiently as STATCOM during nighttime.

5.6 Conclusion

In this chapter, a seamless mode control (SMC) algorithm for a single-stage photovoltaic virtual synchronous generator has been proposed to provide frequency regulation services in case of disturbances and reactive power support in STATCOM mode during the night. Experimental results verify that the proposed algorithm is capable of injecting deloaded power into the grid and maintaining the power reserves. In addition, the proposed method has been tested for varying irradiance conditions and load changes, and satisfactory results have been observed. Further, the frequency regulation capability of the proposed system has been evaluated. It is observed that PV-VSG uses the reserve power to supply the active power proportional to the frequency changes in the case of grid frequency variations without any additional energy storage. During the nighttime, STATCOM mode operation is tested, and results verify the performance of the PV-VSG system with no PV power. In addition, the proposed control algorithm eliminates the requirement of a separate controller for harmonics compensation and for STATCOM mode operation to maintain DC link voltage during the night. A self-synchronization method has been used for the grid connection of PV-VSG. The seamless transition of the proposed PV-VSG is verified by the experimental results.